2011 50th IEEE Conference on Decision and Control and
European Control Conference (CDC-ECC)
Orlando, FL, USA, December 12-15, 2011

Speed and acceleration controllers for a light electric two-wheeled vehicle

Andrea Dardanelli, Mara Tanelli, Bruno Picasso, Sergio M. Savaresi, Onorino di Tanna, Mario Santucci

Abstract— **Environmental concerns and the steadily decreasing oil supplies have promoted a significant interest in electric vehicles (EVs) as a solution for the mobility of the near future, especially in urban environments. The correct handling of the energy behavior on board is one of the most critical problems to be addressed, particularly in urban driving scenarios where the speed profiles – even on fixed routes – are *a priori* unknown since they are affected by significant unpredictable external factors. The high-level control of the energy flows requires an accurate knowledge of the vehicle dynamics, as speed and acceleration directly affect the battery power. To cope with these issues, this paper addresses the modeling and identification of the longitudinal dynamics of an electric two-wheeled vehicle, based on which a model-based motion control strategy is designed. The controller goal is to confine speed and accelerations within desired bounds while guaranteeing a good driving feeling. The approach is experimentally validated on an instrumented light electric two-wheeled vehicle.**

I. INTRODUCTION AND MOTIVATION

The urge to quickly and effectively respond to the need of new solutions for safe and green mobility is being recognized world-wide both from public institutions and from the industrial automotive world, [1], [2]. In this context, recent efforts converge towards electric vehicles (EVs), which seem to be the most promising technology to achieve the needed decrease of greenhouse gas emissions and to form the basis for new models of urban mobility, [3].

As electric and hybrid vehicles are gaining more popularity also among the average consumers, significant research efforts are being devoted to study and design active energy management strategies.

In the hybrid vehicles literature, optimization problems have been defined in order to design optimal strategies for managing the power distribution between the combustion engine and the electric motor so as to achieve fuel consumption minimization, see *e.g.*, [4], [5]. Dedicated modelling efforts have also led to define control-oriented descriptions of the traction dynamics of the vehicles, which are the key ingredients for active controllers tailored to achieve desired levels of energy-efficiency, see *e.g.*, [6], where a dynamic model of the powertrain of hybrid EVs is studied, and [7], which addressed the traction control of an EV.

As far as EVs are concerned the key issue is to design effective controllers that ensure both energy-efficiency and a good driving feeling (two crucial factors to promote the diffusion of such vehicles to the mass market). Further, in view of the fact that energy-consumption, directly related to the battery usage, is first of all affected by the speed/acceleration pattern which the vehicle is subject to, the energy control of such vehicles mainly requires an effective speed and acceleration regulation. Thus, one can ensure that these variables are kept within prescribed limits that derive from higher-level energy-management strategies, [8]. This was confirmed by the energy-profiling efforts discussed in [9], which disclosed that, to ensure the best exploitation of the vehicle energetic capabilities, intermediate speed values were to be preferred and that, for fixed battery discharge rates, the optimal working conditions were confined in a certain region of the speed-acceleration plane.

As such, to enable the design of efficient energy-management strategies, one should first of all be capable of ensuring that speed and acceleration can be regulated and kept within desired bounds while maintaining good driveability. This paper offers a contribution in this direction, proposing a control architecture that achieves these goals. For controller design, a frequency-domain description of the longitudinal vehicle dynamics is identified from *ad hoc* experiments carried out on an instrumented light, electric two-wheeled vehicles. Based on the model, a speed and an acceleration controller are designed, and an appropriate supervisory logic to select the active controller is provided. Further, the tuning phase is outlined. The issue of quantization of the speed measurement is also analyzed, and its effect on closed-loop performance is studied. Finally, the effectiveness of the proposed control strategy is assessed via experimental results.

The structure of the paper is as follows. Section II provides a description of the vehicle set-up, illustrating the measured signals and the data processing steps needed to compute the vehicle acceleration. Section III is devoted to discuss the considered model of the vehicle longitudinal dynamics, and to outline the performed identification tests. Further, Section IV describes the proposed approach for speed and acceleration control, detailing the control architecture and the management of the quantization issues. Finally, Section V presents the experimental results that assess the suitability of the proposed control strategy.

This work was partially supported by MIUR project "New methods for Identification and Adaptive Control for Industrial Systems" and by Piaggio S.p.A.

A. Dardanelli, M. Tanelli, B. Picasso and Sergio M. Savaresi are with Dipartimento di Elettronica e Informazione, Politecnico di Milano, Piazza L. da Vinci 32, 20133 Milano, Italy. E-mail:{dardanelli,tanelli,picasso, savaresi}@elet.polimi.it. O. di Tanna and M. Santucci are with Piaggio & C. S.p.A., Viale Rinaldo Piaggio 25 56025 Pontedera (Pisa), Italy. E-mail:{Onorino.Ditanna, Mario.Santucci}@piaggio.com

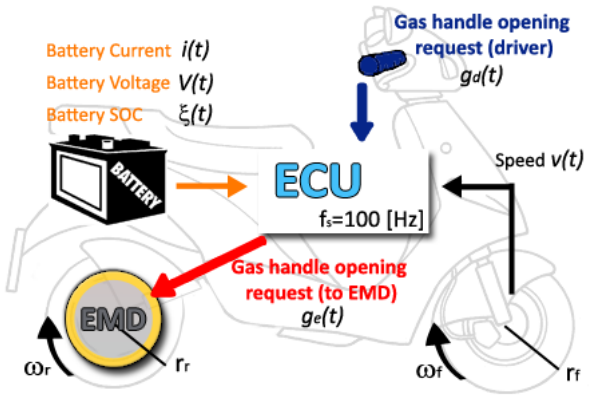

Fig. 1. A schematic representation of the istrumented test vehicle.)

II. VEHICLE SETUP

The test vehicle is a prototype, light two-wheeled electric vehicle equipped with a CAN bus for signal transmission (see Figure 1). The measured signals are the two rotational wheel speeds $\omega_i, i \in \{f,r\}$ and the gas handle opening $g_d(t)$ requested by the rider.

As the considered working conditions for the vehicle are made by urban routes characterized by slow/medium speed and moderate accelerations, the wheel radii can be assumed to be known constants $r_i, i \in \{f,r\}$, see *e.g.* [10], [11]. As such, the vehicle speed $v(t)$ can be computed as $v(t) = \left(\omega_f(t) r_f + \omega_r(t) r_r\right)/2$.

The vehicle is equipped with an electronic control unit (ECU) which reads the signals *via* the CAN bus and is capable of modifying the gas handle opening signal, thus permitting to vary the torque requested to the electric motor and influencing the battery discharge. The electric motor is equipped with an electric motor drive (EMD), which manages its operation. The electric motor transmits traction to the rear wheel *via* a wet transmission. Note that the driver gas request $g_d(t)$ is sent to the vehicle ECU and can be modified. In fact, the main control variable is the actual gas request $g_e(t)$ sent to the electric motor by the ECU, which is a modified version of $g_d(t)$ defined by the controller. Note that $g_e(t)$ is then converted into a current set-point by the EMD via a static map, and such a set-point is tracked by means of a control strategy which is embedded in the EMD itself and thus not known. Further, an estimate of the battery state-of-charge (SoC) $\xi(t)$ is available for future energy control purposes and the battery current $i(t)$ and voltage $V(t)$ are measurable. All signals are sampled at $f_s = 100$Hz. In particular, the available speed measurement v_m is rounded to the nearest integer by the EMD, so that it has a resolution of 1[km/h], while upper (100[%]) and lower (0[%]) limits are applied by the EMD to g_e. It is worth mentioning that the vehicle speed is internally limited to 50km/h.

III. SYSTEM MODELING AND IDENTIFICATION

In this section the model of the vehicle longitudinal dynamics is presented, with the aim of defining the dynamical relation between the gas handle opening $g_d(t)$ (*i.e.*, the model input) and the vehicle longitudinal speed $v(t)$ (*i.e.*, the model output). As a matter of fact, the vehicle control system will be based on vehicle speed and/or acceleration regulation, and it is therefore crucial to get a reliable model of the longitudinal dynamics, for positive values of the speed.

The vehicle forward motion (*i.e.*, for $v > 0$) can be expressed by the following differential equation (see [10])

$$\dot{v}(t) = \frac{1}{M}\left[F_w(t) - \left(F_{br}(t) + F_f(t)\right)\right] \tag{1}$$

where M is the total mass (*i.e.*, the sum of the driver and vehicle masses), F_w is the traction force at the wheel, F_{br} and F_f are the braking force and the friction force, respectively. The latter term can be further expanded as

$$F_f = \frac{1}{2}\rho C_x A v^2(t) + r_v v(t) + F_g(C_r \cos\vartheta(t) + \sin\vartheta(t)) \tag{2}$$

In (2) one can recognize that the friction forces are composed by the sum of the following terms:

- *the aerodynamic drag force*: a quadratic function of the speed. The parameter ρ represents the air density, while C_x and A are the drag coefficient and the reference area of the vehicle, respectively;
- *the viscous force*: a linear function of the speed. This force is mainly due to the oil inside the transmission which links the electric motor and the rear wheel. The 1-dimensional relation between the force and the speed is expressed by means of the damping parameter r_v;
- *the roll and slope forces*: they do not depend on speed, but they are linked by nonlinear relations to the road grade ϑ; the speed-dependent parameter $C_r = C_r(v)$ defines how the gravitational force transmitted to the road $F_g(t) = Mg\cos\vartheta(t)$ is translated into a roll force. For simplicity, we assume this parameter to be constant over the considered range of vehicle velocity.

A nonlinear simplified version of the model can be derived by neglecting the road slope and the braking force, *i.e.*, $\vartheta \approx 0$ and $F_{br} \approx 0$, thus yielding

$$\dot{v}(t) = \frac{1}{M}\left[F_w(t) - \left(\frac{1}{2}\rho C_x A v^2(t) + r_v v(t) + C_r F_g\right)\right] \tag{3}$$

These approximations are not critical, especially in view of the identification experiments that follow, since the experimental tests will be carried out on a flat route. Moreover, the braking force is not measurable on the test vehicle and will be regarded as an unmeasurable disturbance.

The model input, *i.e.*, the gas handle opening $g_d(t)$ is *hidden* within the term F_w; indeed, we can assume that the traction force depends on the gas handle opening, as the torque set-point (*i.e.*, the motor current set-point) computed by the ECU and delivered to the electric motor drive is a function of the angular position of the handle potentiometer.

Model (3) is a nonlinear SISO system, whose input is the gas handle opening $g_d(t)$ and whose output is the vehicle speed $v(t)$. For what follows, we are interested in obtaining a linearized input/ouput model of the longitudinal vehicle dynamics expressed in the frequency domain. To this end, a

frequency sweep of the gas handle opening around a nominal working condition was applied to the system, measuring the output speed. The non-parametric estimate of the frequency response is then estimated using spectral analysis, [12]. Finally, the parameters of the corresponding transfer function were retrieved *via* a weighted least-square algorithm (the weighting has been used to focus the fitting within the range $[0.05, 0.3]$Hz, which proved to be that of interest for controller design), yielding

$$\hat{G}(s) = \frac{\hat{\mu}}{1+s\hat{T}_g} = \frac{0.46}{1+s/(2\,\pi\,0.03)} \tag{4}$$

The transfer function fitting is depicted in Figure 2, in which the experimental data are shown. In order to quantify the quality of the identified model, the mean value of the Error to Signal Ratio (ESR) of the vehicle speed is evaluated for positive accelerations. Denote by v_{id} the output of the identified model, then $ESR(t) = (|v_m(t) - v_{id}(t)|)/(v_m(t))100$. The ESR for the identified linear model turns out to be 3.18%, allowing us to conclude that a single pole linear model provides a good approximation of the system around the nominal working conditions.

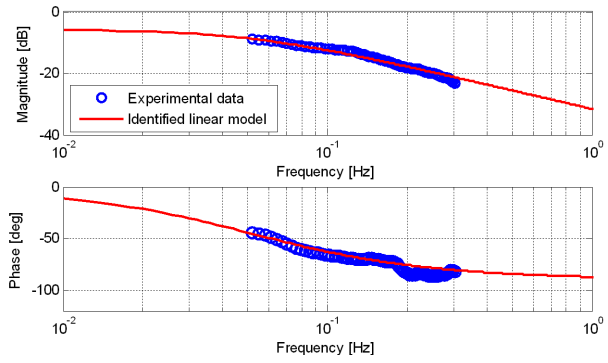

Fig. 2. Magnitude (top) and phase (bottom) of the frequency response: experimental data (circles) and the identified transfer function model (solid line).

Furthermore, an analysis of the linearized vehicle dynamics at different working conditions was performed, based on classical time-domain black-box identification techniques, [13], [14]. The obtained results show that the system pole becomes slower as the speed increases (see Figure 3) while the system gain slightly changes, mainly due to the boost effect which ensures that the vehicle is capable of generating large accelerations at low speed, a crucial property to handle dangerous situations in the urban traffic. Offline validation results are presented in Figure 4, where the measured vehicle speed is compared to the output of estimated linear model around the nominal working conditions. The model is validated just for positive accelerations, since the braking force can not be measured. Hence, during decelerations, the identified speed is made coincident with the measured speed, as can be seen in Figure 4. The results are encouraging, and the performance of the linear model makes it suitable to serve as a basis for control system design.

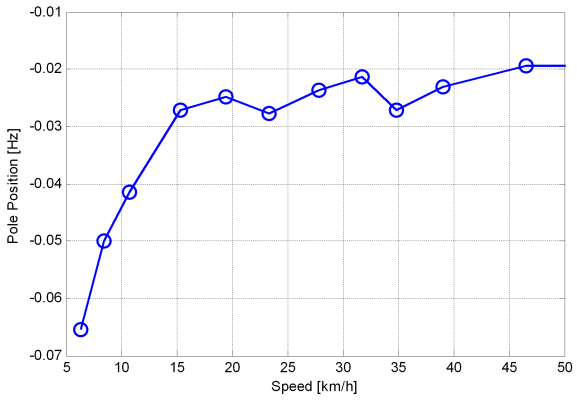

Fig. 3. Plot of the angular position of the pole of the linearized model as a function of speed.

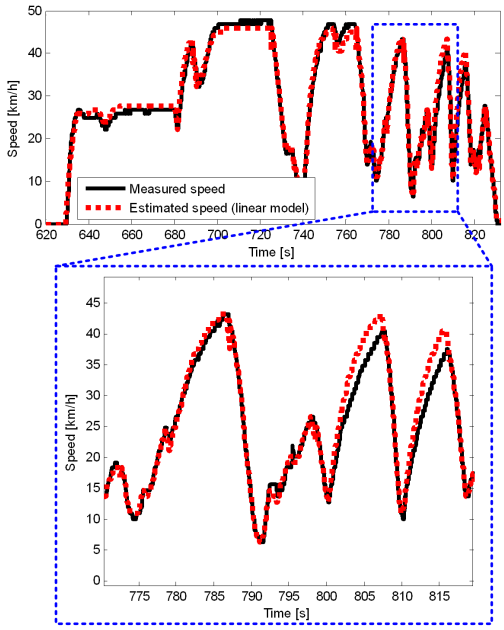

Fig. 4. Time histories of the vehicle speed: measured (solid line), estimated with the nonlinear model (dashed line), estimated with the linear model (dotted line).

IV. VELOCITY AND ACCELERATION CONTROLLERS

The objective of the control system which is presented in this section consists in regulating speed and acceleration so as to limit the dynamical behavior of the vehicle. In particular, the vehicle is automatically controlled when an acceleration bound ($a_b \geq 0$) or a velocity bound ($v_b \geq 0$) is crossed. These bounds are supposed to be slowly varying compared to the longitudinal vehicle dynamics.

The proposed control scheme (see Figure 5) consists of three controllers: the driver D, the acceleration controller R_a and the velocity controller R_v. A supervisory logic handles the transitions between such controllers. Each subsystem is described in the following subsections.

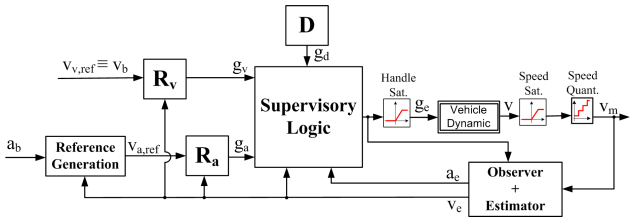

Fig. 5. General schematic of the proposed control strategy.

A. Supervisory Logic

The supervisory logic defines the transitions in accordance with the hereunder described Finite State Machine (FSM) (see also Figure 6). Let g_d, g_a and g_v be the handle provided by D, R_a and R_v, respectively; denote by a_e the estimated acceleration (see Section IV-B), by v_m the measured vehicle velocity and by v_e the estimated vehicle velocity; the active controller, and hence the gas handle opening request g_e actually sent to the EMD, is selected as follows:

- Initialize in the Driver Control State (DCS), thus $g_e = g_d$; remain in the DCS until one of the following conditions holds:
  1) if $[(v_e \geq v_b) \wedge (g_v \leq g_d)]$, switch to the Velocity Control State (VCS), thus $g_e = g_v$;
  2) if $[(a_e \geq a_b) \wedge (g_a \leq g_d) \wedge (v_e < v_b)]$, switch to the Acceleration Control State (ACS), thus $g_e = g_a$.
- If the current state is ACS, remain there until one of the following conditions is satisfied:
  1) if $[(v_e \geq v_b) \wedge (g_a \leq g_d)]$, switch to VCS ($g_e = g_v$);
  2) if $[(g_a > g_d)]$, switch to DCS ($g_e = g_d$).
- If the current state is VCS, remain there until $[(g_v > g_d)]$: in this case, switch to DCS ($g_e = g_d$).

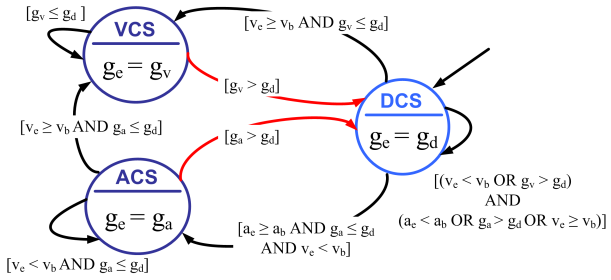

Fig. 6. Finite State Machine modeling the supervisory logic to select the active controller.

Few remarks are in order: from a formal viewpoint, a simple inspection allows one to see that, at each time instant, the current state of the FSM is well-defined (just notice that, if the current state is ACS and both the transitions ACS to VCS and VCS to DCS are active, thus $v_e \geq v_b$, then the state switches to DCS and remains therein because, being $v_e \geq v_b$, the transition DCS to ACS is not active). The FSM is supposed to be discrete-time driven (the signals are sampled at 100Hz), therefore Zeno behaviors are not an issue, see *e.g.*, [15]. Nevertheless, in the presence of particular and uncommon behaviors of the signal g_d (such as a high frequency sinusoidal signal), it is possible that a fast switching between DCS and VCS or between DCS and ACS occurs. This phenomenon can be avoided by enforcing a dwell-time in the DCS. Notice also that no transition from VCS to ACS is provided because, under velocity regulation, acceleration tends to zero and incidental violations of the acceleration bound are only possible during short time intervals in the transient behavior. Let us finally notice that safety-critical problems are (at least partially) handled by the conditions ensuring that the automatic controllers R_a and R_v are disabled as soon as they provide a larger handle request (g_a and g_v, respectively) than the driver one g_d (see the red arches in Figure 6). In particular, the driver takes control of the vehicle whenever he/she requests a deceleration. It is also worth mentioning that, by properly selecting the speed and acceleration bounds, one can guarantee an acceptable acceleration of the vehicle at low speeds, which is necessary for safety guarantees, *e.g.*, for avoiding obstacles).

B. Observer and Estimator

The measured speed v_m is affected by a significant quantization noise, due to the limited number of teeth of the wheel encoder; this nonlinearity represents a significant issue for control purposes: indeed, a reduced closed-loop bandwidth (lower than or equal to that of the identified open-loop system) is needed in order to cope with the ripples on the control variable caused by the quantization of v_m; these ripples can be perceived by the driver, causing significant discomfort and a bad driving feeling. Moreover, a real-time estimation of the acceleration based on the measured vehicle speed requires a filtering process whose induced phase-shift is not negligible, thus resulting in a not satisfactory tracking of the acceleration reference; hence, a regularization of the vehicle speed measurement is essential. An effective viable approach to this issue is to reconstruct the vehicle speed v adopting the following extended Luenberger observer, [16]

$$\begin{cases} \dot{\hat{x}}(t) &= \hat{A}\hat{x}(t) + \hat{B}g_e(t) + \Gamma_1(v_m(t) - v_e(t)) + \Gamma_2\eta(t) \\ \dot{\eta}(t) &= v_m(t) - v_e(t) \\ v_e(t) &= \hat{C}\hat{x}(t), \end{cases} \tag{5}$$

where $(\hat{A}, \hat{B}, \hat{C})$ are the matrices (scalars in our case) of a state-space realization of the identified model (4). The additional component η allows one to guarantee that the estimated speed v_e converges to the quantized one v_m when g_e is constant (*i.e.*, in steady-state): this is a necessary condition to ensure the correct tracking of slowly varying speed bounds since it limits the steady-state estimation error when the modeling errors are not negligible. In fact, if $v(t)$ is constant then

$$|v_m(t) - v(t)| \leq 0.5 \Rightarrow \tag{6}$$

$$\Rightarrow \limsup_{t \to +\infty} |v_e(t) - v(t)| \leq e_{q_M} = 0.5\text{km/h}, \tag{7}$$

where $e_{q_M} = 0.5$km/h is the maximum quantization error with the considered wheel encoders. The acceleration a_e is then estimated by numerical differentiation of the estimated speed

v_e. The tunable parameters Γ_1, Γ_2 determine the observer dynamics and have been selected based on experimental data.

C. Computation of the Reference Signals

While the speed bound v_b directly defines the internal set-point of the velocity controller, the reference signal for the acceleration control loop is generated according to the following logic

$$v_{ref}(t) = \begin{cases} v_e(t_0) + \int_{t_0}^{t} a_b(t)dt, & \text{ACS active} \\ v_e(t), & \text{ACS not active} \end{cases} \quad (8)$$

where t_0 is the time instant at which a transition to the ACS occurs.

The adopted policy for the acceleration set-point generation is such that the acceleration controller, when active, tracks a speed ramp. This solution is appealing since the feedback loop employs the regularized speed v_e instead of the acceleration estimate a_e, so that the control variable g_a does not oscillate even if the closed-loop bandwidth is larger than the open-loop one.

D. Speed and Acceleration Controllers

PI controllers are adopted for both velocity and acceleration loops, *i.e.*,

$$R_v(s) = K_{p,v}\left(1 + \frac{1}{sT_{i,v}}\right) \quad (9)$$

$$R_a(s) = K_{p,a}\left(1 + \frac{1}{sT_{i,a}}\right). \quad (10)$$

The configuration implemented on board of the vehicle is depicted in Figure 7 for the case of the acceleration controller R_a; the following considerations are made for the acceleration controller but they can be seamlessly extended to the speed controller, as the same strategy is adopted.

The PI controller is endowed with anti-windup capabilities, due to the presence of a saturation on the gas handle opening. Furthermore, a feedforward action g_f guarantees a faster response of the closed-loop system. Notice that the speed reference is weighted with $1/\hat{\mu}$ (where $\hat{\mu}$ is the DC gain of the identified transfer function (4), while μ denotes the unknown nominal DC gain value); if $\hat{\mu} \approx \mu$, the magnitude of the feedforward action depends on the distance between the steady-state gas handle opening at speed $v_e(t_0)$ and the actual gas handle opening $g_e(t_0)$, t_0 being the switching time instant.

Note that the controller architecture (see Figure 7) guarantees bumpless transfer, *i.e.*, if the "switch on" of the controller occurs at time t_0, then $g_e(t_0^-) \approx g_e(t_0^+)$ (see [17]). It is important to point out that, thanks to the adopted policy for the set-point computation given in (8), $e(t_0) = 0, g_f(t_0) = 0$. Moreover, by inspecting Figure 7, it is easy to see that, when the control is switched off, g_{PI} tracks g_e with an error dynamics determined by T_t. From these considerations we can conclude that, by properly selecting the parameter T_t, we can force the desired bumpless behavior, *i.e.*,

$$\left.\begin{array}{l} g_a(t_0^-) = g_a(t_0^+) = g_e(t_0^+) \\ g_a(t_0^+) \approx g_e(t_0^-) \end{array}\right\} \Rightarrow g_e(t_0^-) \approx g_e(t_0^+) \quad (11)$$

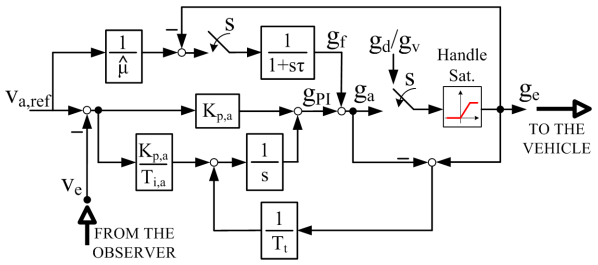

Fig. 7. Schematic representation of the R_a controller. The switching signal s activates the control loop according to the rules specified by the supervisory logic.

V. EXPERIMENTAL RESULTS

The controller parameters have been tuned in order to achieve a closed-loop bandwidth of approximately 0.3Hz. Since the acceleration control action is more critical from the comfort perspective (see *e.g.*, [18], [19]), the bandwidth of the acceleration controller is slightly lower than that of the speed controller: this choice leads to a better driver feeling when the acceleration limit is very low and the vehicle accelerates at low speeds. Indeed, by doing this, the acceleration will cross the bound for a certain amount of time that depends on closed-loop bandwidth of the related control system, until the PI integral action makes the error go toward zero. This slower transient behavior enhances the driveability of the vehicle in an urban scenario, where large accelerations at low speeds have to be made possible for managing potentially dangerous situations.

To assess the validity of the proposed controllers, two kinds of results are presented:

- experimental tests with constant speed and acceleration bounds (see Figure 8);
- experimental tests with slowly varying speed and acceleration bounds (see Figure 9);

For the constant bound case, the state of the FSM is also depicted. In the tests, the bounds are supposed to belong to the intervals $a_b \in [0,4]$ m/s^2 and $v_b \in [30,50]$ km/h. By inspecting the figures, the reader can appreciate the bumpless transfer and the effective management of the interaction between the two controllers. As previously explained, the acceleration crosses its bound at low speed. A final remark is devoted to the case with a slowly varying acceleration bound (see Figure 9). Notice that this bound has been selected as a monotonically decreasing function of the filtered speed v_e: for energy management purposes this choice is quite typical; indeed, as the speed increases, the inertial power becomes comparable to the friction losses. As a consequence, limiting the acceleration has an effective impact on the decrease of the energy consumption.

VI. CONCLUSIONS AND FUTURE WORK

This paper presents a control strategy for a light electric two-wheeled vehicle aimed at ensuring that speed and acceleration remain within prescribed bounds. To guide controller

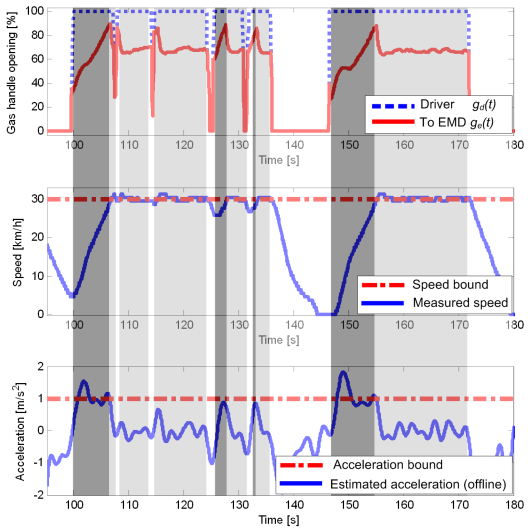

Fig. 8. Experimental results for the constant speed and acceleration bounds ($a_b = 1[\mathrm{m/s^2}]$, $v_b = 30[\mathrm{km/h}]$). Top plot: time history of the gas handle opening. Driver request (dotted line) and $g_e(t)$ solid line. Middle plot: time history of the vehicle speed. Speed bound (dash-dotted line) and measured speed (solid line). Bottom plot: time history of the vehicle acceleration. Acceleration bound (dash-dotted line) and measured acceleration (solid line). White background: driver control; light gray background: velocity control; dark gray background: acceleration control.

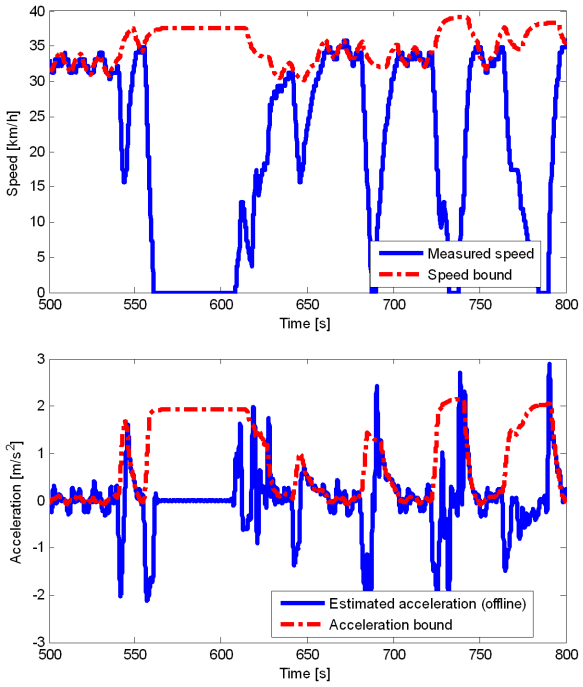

Fig. 9. Experimental results for the slowly varying speed and acceleration bounds. Top plot: time history of the vehicle speed. Speed bound (dash-dotted line) and measured speed (solid line). Bottom plot: time history of the vehicle acceleration. Acceleration bound (dash-dotted line) and measured acceleration (solid line).

tuning, the model of the longitudinal vehicle dynamics has been derived via frequency-domain identification tests. A solution to alleviate the significant quantization affecting the speed measurement has been proposed, and the effect of the ripple on the control variable has been minimized while guaranteeing an acceptable bandwidth for the closed-loop system. Future developments shall include the quantitative analysis of the existing trade-off between driver comfort and regulation performance. The information conveyed by the velocity at which the gas handle is open will be introduced in the control architecture to enhance the safety of the overall system. Moreover, the main focus will be on devising a high-level energy management strategy which defines on-line the most appropriate bounds on speed and acceleration based on energy-consumption considerations.

REFERENCES

[1] E.U.Commission, "Greening road transport: Eu-funded research supports eu's environmental objectives," memo/09/26, Brussels, 26 January 2009.

[2] F. Hacker, R. Harthan, F. Matthes, and W. Zimmer, "Environmental impacts and impact on the electricity market of a large scale introduction of electric cars in europe," eTC/ACC Technical Paper 2009/4.

[3] C. Chan, "The state of the art of electric and hybrid vehicles," *Proceedings of the IEEE*, vol. 90, no. 2, pp. 247–275, 2002.

[4] A. Sciarretta, M. Back, and L. Guzzella, "Optimal control of parallel hybrid electric vehicles," *IEEE Transactions on Control Systems Technology*, vol. 12, no. 3, pp. 352–363, 2004.

[5] F. Salmasi, "Control strategies for hybrid electric vehicles: Evolution, classification, comparison, and future trends," *IEEE Transactions on Vehicular Technology*, vol. 56, no. 5, pp. 2393–2404, 2007.

[6] B. Powell, K. Bailey, and S. Cikanek, "Dynamic modeling and control of hybrid electric vehicle powertrain systems," *IEEE Control Systems Magazine*, vol. 18, no. 5, pp. 17–33, 2002.

[7] Y. Hori, Y. Toyoda, and Y. Tsuruoka, "Traction control of electric vehicle: Basic experimental results using the test EV UOT Electric March," *IEEE Transactions on Industry Applications*, vol. 34, no. 5, pp. 1131–1138, 2002.

[8] C. Lin, H. Peng, and J. Grizzle, "A stochastic control strategy for hybrid electric vehicles," in *Proceedings of the 2004 American Control Conference*, vol. 5, Boston, Massachusetts, 2005, pp. 4710–4715.

[9] A. Dardanelli, M. Tanelli, B. Picasso, S. M. Savaresi, O. Di Tanna, and M. Santucci, "Control-oriented energy-profiling and modelling of urban electric vehicles," in *Proceedings of the 2011 Multiconference on Systems and Control*, Denver, CO, 2011, submitted.

[10] U. Kiencke and L. Nielsen, *Automotive Control Systems*. Springer, Berlin, 2000.

[11] H. B. Pacejka, *Tyre and Vehicle Dynamics*. Oxford: Buttherworth–Heinemann, 2002.

[12] P. Wellstead, "Non-parametric methods of system identification," *Automatica*, vol. 17, no. 1, pp. 55–69, 1981.

[13] L. Ljung, *System Identification: Theory for the User*. Prentice-Hall, Upper Saddle River, NJ, 1999.

[14] T. Söderström and P. Stoica, *System Identification*. London: Prentice Hall, 1989.

[15] M. Heymann, F. Lin, G. Meyer, and S. Resmerita, "Analysis of Zeno behaviors in a class of hybrid systems," *IEEE Transactions on Automatic Control*, vol. 50, no. 3, pp. 376–383, 2005.

[16] D. Luenberger, "An introduction to observers," *IEEE Transactions on Automatic Control*, vol. AC-16, no. 6, pp. 596–602, 1971.

[17] K. Astrom and T. Hagglund, "PID Control, The control handbook," 1996.

[18] *Mechanical vibration and shock evaluation of human exposure to whole-body vibration part 1: general requirements*, ISO, 1997, iSO 2631-1.

[19] D. Hrovat and M. Hubbard, "A comparison between jerk optimal and acceleration optimal vibration isolation," *Journal of Sound and Vibration*, vol. 112, no. 2, pp. 201–210, 1987.